Quarterly Journal of the Royal Meteorological Society Q. J. R. Meteorol. Soc. 136: 2176–2188, October 2010 Part B

The formation of a multicell thunderstorm behind a sea-breeze front

Ulrike Wissmeier,* Roger K. Smith and Robert Goler
Meteorological Institute, University of Munich, Germany
*Correspondence to: Ulrike Wissmeier, Meteorological Institute, University of Munich, Theresienstrasse 37, 80333 Munich, Germany. E-mail: ulrike@meteo.physik.uni-muenchen.de

Idealized three-dimensional numerical simulations are used to investigate the influence of sea breezes on the evolution of multicell thunderstorms in the Tropics. The study is motivated by a desire to understand a particular type of severe storm system that occurs occasionally over the 'Top End' region of northern Australia, but the results should have wider applicability. The calculations are carried out using Bryan's cloud model.

The simulations reproduce the main features of the evolution of an observed storm system. New cells develop on the gust front of the initial updraught, behind the sea-breeze front, and subsequently merge to form a multicell thunderstorm. The propagation speed and direction, the orientation, and length of the line of updraught cells are all similar to those observed. The sea breezes in the model play an important role in the evolution of the storm. In general, the low-level convergence at the gust front produced by the initial cell needs to be strong enough and to persist for a sufficiently long time to allow new cells to develop near this front. A strong cold pool occurs if the initial updraught is sufficiently tilted so that the downdraught does not fall into it, but supplies cold air close to the gust front. A generalized form of the Rotunno–Klemp–Weisman criterion was used to test whether the new updraughts developed at locations where the cold pool circulation was largely opposed by that of the environmental shear. The comparison of the shear components normal to the gust front showed that new cells develop even though this criterion is not fulfilled, suggesting that the criterion is not applicable to the more complex flow configurations studied here.

Key Words: deep convection; Tropics; multicell thunderstorm; gust front; squall line; severe weather

Received 31 August 2009; Revised 5 July 2010; Accepted 28 July 2010; Published online in Wiley Online Library 7 October 2010

Citation: Wissmeier U, Smith RK, Goler R. 2010. The formation of a multicell thunderstorm behind a sea-breeze front. *Q. J. R. Meteorol. Soc.* **136**: 2176–2188. DOI:10.1002/qj.691

1. Introduction

Sea breezes occur in many coastal regions of the world and result from temperature differences between the land and sea. The temperature contrast leads to onshore flow if the offshore component of the broadscale flow is not too strong. Sea breezes in the middle latitudes can be particularly strong in summer when the land is heated strongly, but at lower latitudes they can be strong at any time of the year. Observational and numerical studies of sea and land breezes in the Tropics have shown that the convergence and lifting they produce can trigger thunderstorms (e.g. Keenan and Carbone, 1992; Carbone *et al.* 2000; Wapler and Lane, 2010). In their study of convection in the Darwin region of northern Australia, Keenan and Carbone (1992) found that the initial convective cells tend to evolve towards a line of thunderstorms, which is oriented perpendicular to the low-level shear and shows squall-line characteristics.

A particular type of multicell thunderstorm or squall line that occurs occasionally in the Darwin region and which can be severe is the so-called 'Northeaster', which owes its name to the direction from which it moves. Darwin (12°S, 131°E; Figure 1) is a coastal city lying in the 'Top End' of Australia and experiences, on average, 80 days of thunder each year. This study is motivated by a desire to understand the effects of the local sea breezes on the development of the Northeaster.

A good example of a Northeaster is the storm that passed over Darwin during the afternoon of 14 November 2005. The automatic weather station at the airport was hit by lightning and ceased recording during the storm. Trees were uprooted or snapped along a 1 km stretch of the highway adjacent to the airport, the outward-bound section of the highway was blocked, and power supplies were disrupted. The formulation of the idealized numerical calculations described herein is motivated by the radar observations relating to this storm.

Forecasters have speculated that the local sea breezes play an important role in the evolution of Northeasters, but there does not appear to be any research to support this hypothesis, or that might help to understand the evolution of this type of storm system. Nevertheless, there are some studies of moist convection related to sea breezes. Rao and Fuelberg (2000) investigated deep convection behind the Cape Canaveral sea-breeze front using a three-dimensional numerical model. They found that, where storm development was suppressed by subsidence from a neighbouring cell, a new storm developed when surface lifting was provided by an outflow boundary. They argued that Kelvin–Helmholtz instability behind the sea-breeze front can be critical in determining the location and time of storm development. Kingsmill (1995) examined the initiation of convection associated with the collision of a sea-breeze front and a gust front using observational data collected in summer months in Florida. He found that inflections or kinks in boundary-layer convergence zones can be preferred areas for the initiation of deep convection. Neither of these studies addressed the role of the low-level vertical wind shear provided by the sea breeze and their region of interest lay outside the Tropics.

There have been many numerical studies of the dynamics of midlatitude thunderstorms. Three of particular relevance to the present investigation are those of Rotunno *et al.* (1988), Weisman *et al.* (1988), and Weisman and Rotunno (2004), which examined the role of the cold pool and low-level shear on the structure and evolution of deep convection. These authors concluded that the relationship between the low-level shear generated by the cold pool and that associated with the environmental wind is 'the most fundamental internal control on squall-line structure and evolution'. A particular finding was that, in an environment without vertical wind shear, a density current leads to an updraught which is tilted towards its rear due to the influence of the horizontal roll vortex at the edge of the cold pool (Rotunno *et al.*, 1988, Figure 18). However, the circulation associated with the horizontal vorticity of the cold pool can balance that associated with the opposite-signed vorticity of the low-level environmental wind shear. This balance results in deep lifting at the nose of the outflow, and thus in an updraught that is vertical.

Rotunno *et al.* proposed the following criterion for the ability of a cold pool to produce a vertical updraught:

$$\Delta u = c_{\text{pool}}, \tag{1}$$

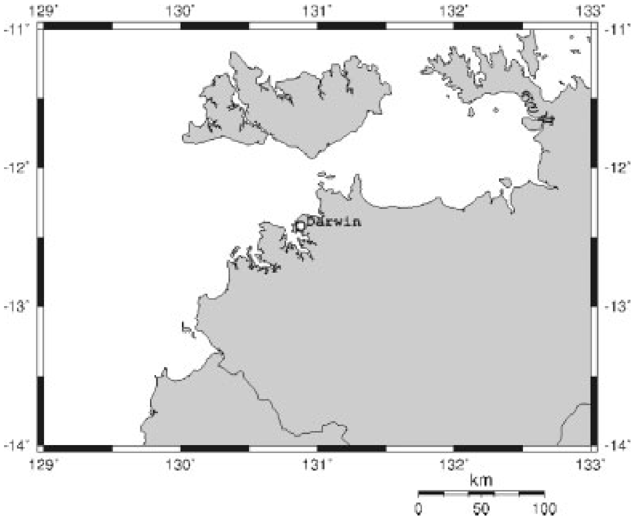

Figure 1. Geography near Darwin, Northern Territory, Australia.

where Δu represents a vertical wind difference characterizing the low-level environmental shear and c_{pool} is the theoretical speed of propagation of a two-dimensional density current given by:

$$c_{\text{pool}}^2 = 2\int_0^H (-B)\,\mathrm{d}z, \tag{2}$$

where H is the depth of the cold pool, and B is the buoyancy of the cold air relative to its environment. We refer to Eq. (1) as the Rotunno–Klemp–Weisman (RKW) criterion. Another way of viewing this criterion is that a cell triggered by a cold pool can realize its full potential only when the cold-pool circulation is largely opposed by that of the shear.

The foregoing studies used idealized wind profiles to investigate the influence of environmental vertical wind shear on deep convection. However, to our knowledge, the applicability of the RKW criterion to cases where the environmental wind shear vector turns with height and where a sea-breeze flow modifies the wind structure at low levels remains to be determined.

This paper presents idealized numerical simulations relevant to the Northeasters, and in particular to the severe event that occurred on 14 November 2005. The broad aim is to try to understand the role of the environmental vertical wind shear on the evolution of this storm, based on the simulations. Particular aims are to examine how the additional lifting and low-level vertical wind shear provided by the sea breeze lead to the formation of a severe multicell storm and to determine the utility of the RKW criterion for understanding these storms. The observations acquired for the 14 November case serve as a reality check on the simulated storms.

The paper is organised as follows. First, in section 2, we review briefly the numerical cloud model and the model configuration and parameters used to simulate the Northeaster. The model results are compared with observations and interpreted in sections 3 and 4, and the conclusions are drawn in section 5.

2. Model configuration

The simulations to be described use the three-dimensional, non-hydrostatic cloud-scale model of Bryan and Fritsch

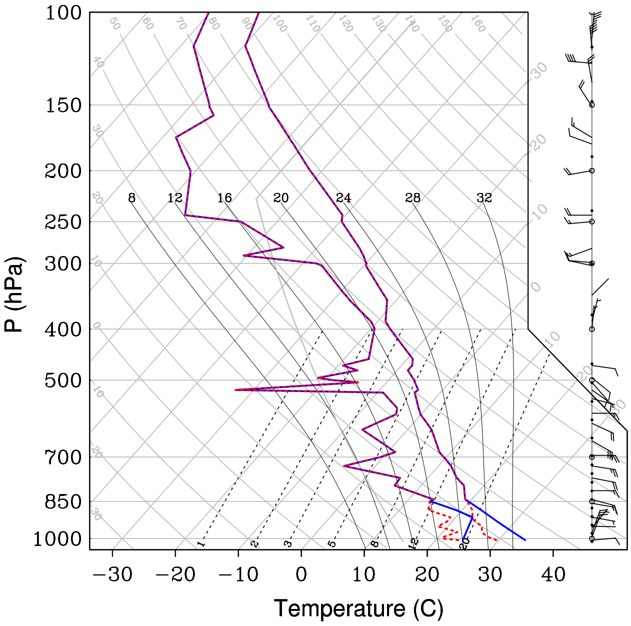

Figure 2. Skew T–log p diagram showing the temperature and dew-point temperature of the Darwin airport sounding at 0000 UTC on 14 November 2005, as used in the simulations (solid lines) and unmodified (dashed lines). Every second wind barb is plotted on the right. 0000 UTC corresponds to 0930 h local time. This figure is available in colour online at wileyonlinelibrary.com/journal/qj

(2002) and Bryan (2002) with the ice microphysics scheme included. This scheme is identical to Gilmore's Li-scheme, where cloud water, rain water, cloud ice, snow, and hail/graupel are predicted (Lin *et al.*, 1983; Gilmore *et al.*, 2004).

Convection is initialised in an environment with vertical profiles of wind, temperature, and moisture taken from the Darwin sounding at 0000 UTC on 14 November 2005 (Figure 2). To represent the mid-afternoon conditions when the Northeaster on this day developed, the lowest 1 km of the sounding is modified to give a convectively mixed boundary layer where $\theta_0 = 306.75$ K and $q_{v0} = 19.34\,\mathrm{g\,kg^{-1}}$ (Figure 2, solid lines). The values for θ_0 and q_{v0} are chosen to coincide with the data recorded at 1 min intervals at Darwin airport. The calculated Convective Available Potential Energy (CAPE)* based on these values is $4129\,\mathrm{J\,kg^{-1}}$. While this value might seem large compared to those found for midlatitude environments of severe thunderstorms (e.g. Weisman and Klemp, 1982), it is appreciably less than the CAPE calculated by the Darwin Regional Forecasting Centre for the 14 November sounding, which is $5069\,\mathrm{J\,kg^{-1}}$.

The model has a domain size of $90 \times 60 \times 28\,\mathrm{km^3}$, with a horizontal grid spacing of 1 km. The vertical grid is stretched from 120 m at the bottom of the domain to 1 km at the top to improve the numerical resolution near the surface, where it is most needed. Convection is triggered by an axisymmetric thermal perturbation of horizontal radius 4 km and vertical extent 1000 m. The temperature excess is 2 K at the centre of the thermal and decreases gradually to zero at its boundary.

A number of experiments is performed with a combination of a northerly (Nsb), westerly (Wsb), and/or a northwesterly sea breeze (NWsb). The configuration of the experiments is shown in Figure 3 and will be explained later in more detail. Each sea breeze is initialised using a box of cold air in the north, west, and/or northwest of the domain at the beginning of the simulation. The locations of the cold boxes are chosen to reflect the orientation of the coastline around Darwin (Figure 1). The potential temperature of a northerly sea breeze with its front located at $y = y_{\mathrm{north}}$, for example, is given by

$$\theta = \theta_{\mathrm{sb}}\left(\frac{z_{\mathrm{sb}} - z}{z_{\mathrm{sb}}}\right) \quad \text{for } y > y_{\mathrm{north}} \text{ and } z < z_{\mathrm{sb}},$$

where θ_{sb} is the temperature excess and z_{sb} the depth of the cold box. Values of $z_{\mathrm{sb}} = 2$ km and $\theta_{\mathrm{sb}} = -2$ K are chosen, based on observations of sea breezes in the Darwin region (Todd Smith, Darwin Regional Forecasting Centre, personal communication; May *et al.*, 2002). While the initial wind fields are horizontally homogeneous (Figure 2), the cold sea-breeze air flows as a density current away from its region of origin, i.e. towards the south, southwest, or east, depending on the initial orientation of the cold-air boundary. Each experiment is run for 180 min to provide adequate time for the initial updraught and the subsequent storm system to develop.

3. The basic experiment

To create environmental conditions similar to those on 14 November 2005, the model is initialized with two cold boxes representing the northerly and northwesterly sea breezes. A warm bubble is placed slightly ahead of the northerly sea-breeze front (Figure 3) so that the first updraught develops directly above it, thereby simulating convection triggered by this sea breeze. This model run will be referred to below as the 'basic experiment'.

3.1. Initial cell

Horizontal cross-sections through the initial cell† and the subsequent storm system at mid-levels are shown in Figure 4 at times $t = 30$, 50, 70, and 110 min. The northerly and northwesterly sea-breeze fronts are depicted by dotted lines, while the gust front is marked by the thick black contour. Regions of ascent are shaded. The corresponding low-level storm structure is shown in Figure 5. The model output illustrated in these figures will be compared now with the radar pictures from 14 November 2005 and with the Severe Thunderstorm report for this event, which was published by the Regional Forecasting Centre in Darwin.

At 0100 UTC on 14 November 2005, the northerly sea breeze along the north coast and the westerly sea breeze along the west coast began to move inland. At 0130 UTC, the northwesterly sea breeze moved over Darwin airport. The first cell formed on the northerly sea-breeze front at 0310 UTC, which corresponds with a model time of about 30 min. These conditions were created 'artificially' in the model as described above and depicted in Figure 3 (basic). The northerly and northwesterly sea breezes propagate southwards and southeastwards, respectively, and the initial

*CAPE is calculated here from the model output, using Bryan and Hart's skew T program, where pseudoadiabatic processes and Bolton's formula (Eq. (43) in Bolton, 1980) for equivalent potential temperature are used.

†The terms 'cell' and 'updraught' are used here as synonyms and represent convection in the form of a single updraught.

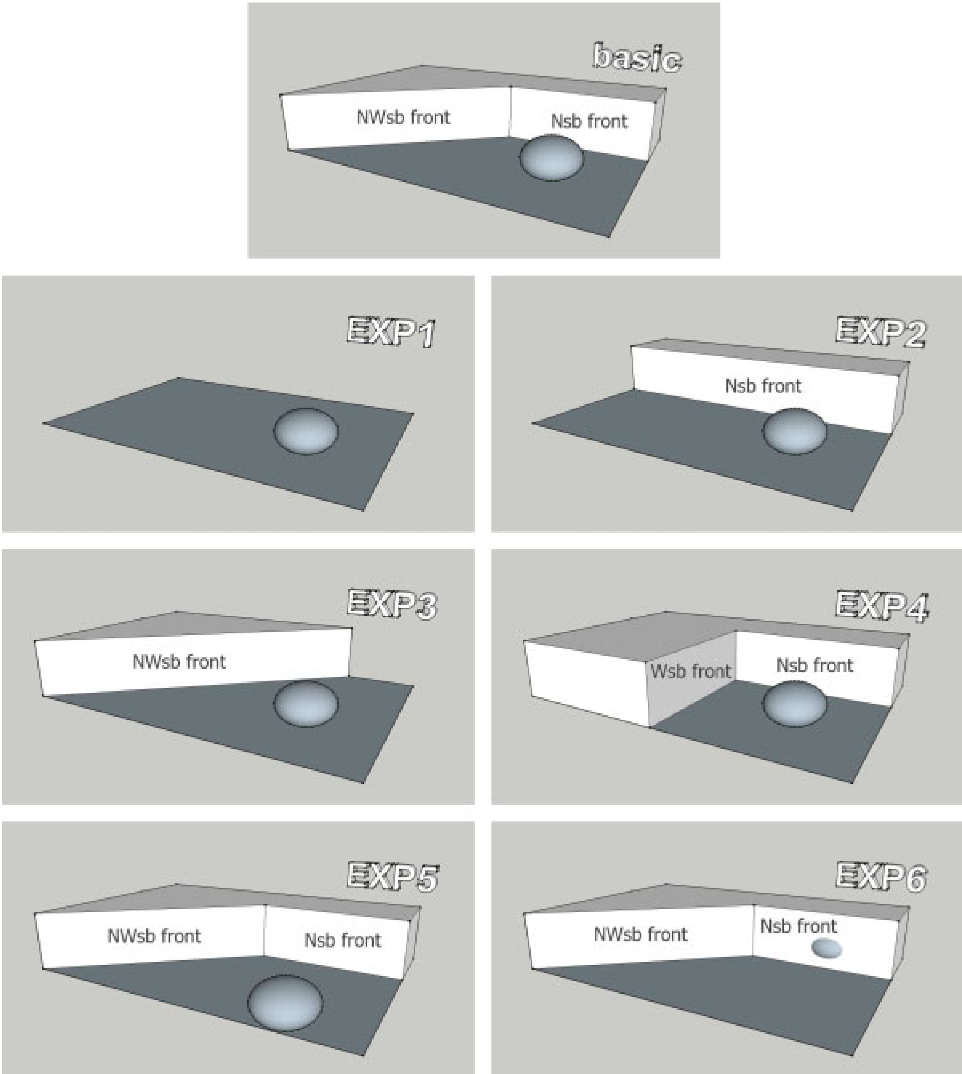

Figure 3. Schematics showing the configuration of the basic experiment and Experiments 1 to 6. The view is from the southsoutheast. The dark grey surface represents the model domain, the boxes represent the sea breezes being 2 K colder than the environment, and the bubble represents the thermal perturbation being 2 K warmer than the environment. This figure is available in colour online at wileyonlinelibrary.com/journal/qj

cell forms on the northerly sea-breeze front (Figure 4(a)). The updraught of this cell attains a maximum speed of 28 m s^{-1} after 48 min.

The early radar pictures (not shown) indicate that the initial cell progressed to the west, along the sea-breeze boundary, with a speed of about 9.4 m s^{-1}. At 0350 UTC, the cell met the northwesterly sea breeze and collapsed, creating a spreading gust front. The westward movement of the initial cell was captured also by the model as seen by comparing Figures 4(a) and (b), although the propagation speed is a little less than one half of that observed. This westward movement is a result of the environmental easterly winds at low- and mid-levels. The gust front forms at $t_{gf} = 42$ min and leads to large horizontal convergence at its northern and western edges (Figure 5). The initial updraught decays after about 60 min as it becomes cut off from the warm environmental inflow by the expanding gust front. The lifetime of this cell is similar to that observed. The Severe Thunderstorm report speculates that the cell decayed as it interacted with the northwesterly sea breeze, although it is not possible to verify this inference from the available observations.

3.2. *Multicell development*

New cells were observed to develop on the gust front of the initial updraught, parallel to, but behind, the northerly sea-breeze front. In the model, the first new updraught forms at the northwestern edge of the gust front after 66 min (Figure 4(c)). At this time, the surface convergence ahead of the cold pool is large in the region where this cell is triggered (Figure 5(c)). New cell development continues to occur behind the sea-breeze front as observed in the radar images.

According to the Severe Thunderstorm report, the system had developed into a multicell complex at 0420 UTC, corresponding to a model time of about 100 min. Figure 6 shows a radar image of the Darwin region at 0420 UTC on 14 November 2005, where the northerly and northwesterly sea-breeze fronts are marked by thin lines of reflectivity (indicated by arrows in the figure). Both the southward- and southeastward-moving sea breezes have triggered strong convection already, and the Northeaster is apparent northeast of Darwin (D). At this time the thunderstorm system in the model (Figure 4(d)) has the structure of a multicell storm. A multicell storm is defined here as a short

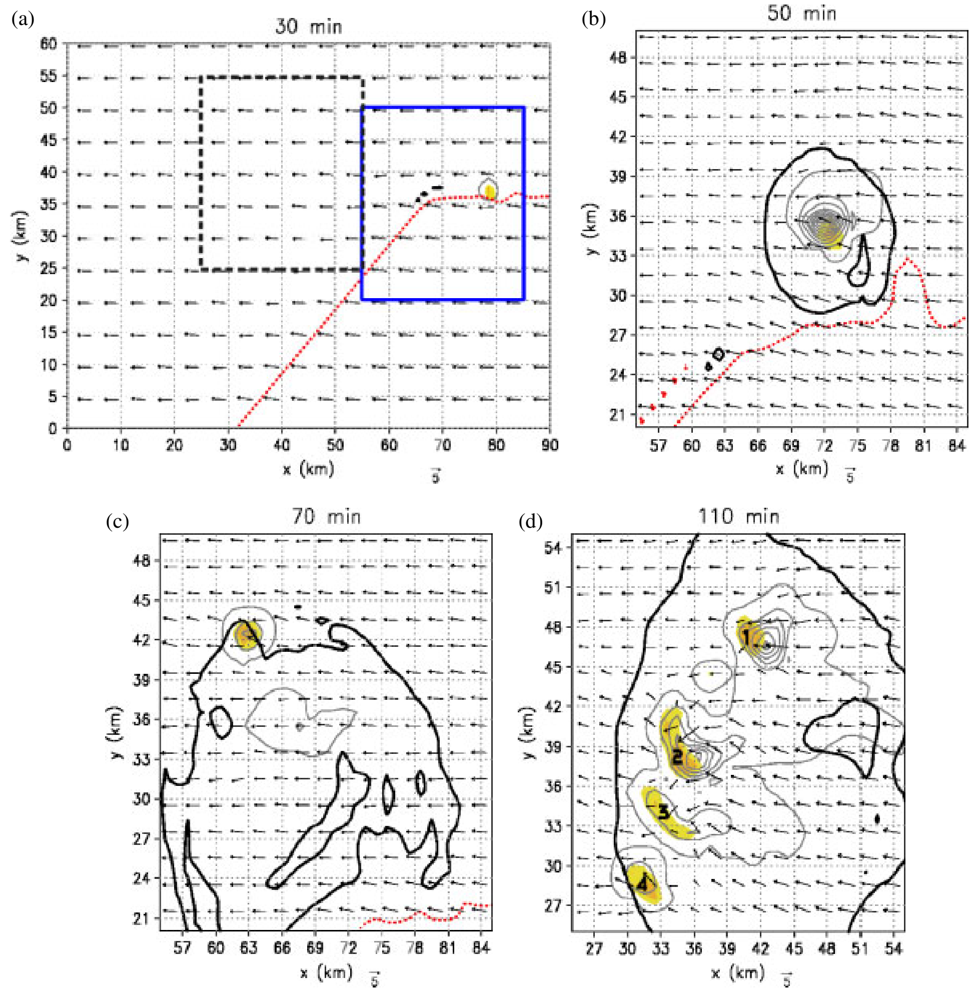

Figure 4. Mid-level storm structure depicted at t = (a) 30, (b) 50, (c) 70 and (d) 110 min. The sea-breeze fronts and the gust front are denoted by the bold dotted and solid lines, respectively, and represent the −0.5 K temperature perturbation contour. Vectors represent horizontal flow at $z = 4.6$ km, and the total precipitation (rain, snow, hail/graupel) mixing ratio, $q_n = q_r + q_s + q_g$, is contoured in grey at 2 g kg^{-1} intervals, with the zero contour omitted. Regions of updraught velocities at $z = 4.6$ km larger than 5 m s^{-1} and 10 m s^{-1} are shaded. (a) shows the whole model domain, (b) and (c) depict expansions of the solid box in (a), and (d) of the dashed box in (a). In (d), the first, second, third and fourth new cells are marked by the respective numbers. This figure is available in colour online at wileyonlinelibrary.com/journal/qj

squall line composed of at least two updraughts with vertical velocities exceeding 5 m s^{-1} at any stage of their life cycle and with the distance between neighbouring updraughts being less than 10 km.

The observed multicell storm propagated towards the westnorthwest, at a speed of approximately 40 km h^{-1}. New cells were generated along the southern flank of the system gust front and the complex became aligned northnortheast/southsouthwest. In the model, the storm system moves also towards the westnorthwest with a speed of about 39 km h^{-1}. New cells develop along the gust front, south of the complex, leading to an alignment of the individual cells from northnortheast to southsouthwest (Figure 4(d)). Thus, the line of convection is oriented perpendicular to the low-level shear vector. This orientation was found also in observational studies by Keenan and Carbone (1991), where it was observed consistently with all types of convection (monsoonal system convection, sea-breeze convection, squall lines).

The basic experiment shows that, with a single warm bubble and two cold boxes that are initialised at the right time and position, a multicell storm develops with similar characteristics to that of 14 November 2005. The simulation compares well with reality in the following respects:

- The initial cell progresses towards the west;
- New cell development occurs on the gust front of the initial cell leading to the formation of a multicell storm;
- The new cells develop behind the sea-breeze front along the southern flank of the multicell storm;
- The translation speed and direction of the line of updraughts is 40 km h^{-1} to the westnorthwest;
- The orientation of the storm system (northnortheast/southsouthwest); and
- The length of the convective line (25 to 30 km).

4. Sensitivity experiments

We investigate now the role of the two sea breezes in the evolution of the multicell thunderstorm on 14 November 2005 by modifying the basic experiment. Six sensitivity experiments are examined. The configuration of these is shown schematically in Figure 3. In the first four experiments (1–4) we examine the importance of the sea breezes: Experiment 1 has no sea breezes; Experiment 2 has only a northerly sea breeze; Experiment 3 has only a northwesterly sea breeze; and in Experiment 4, the northwesterly sea breeze is replaced by a westerly sea breeze.

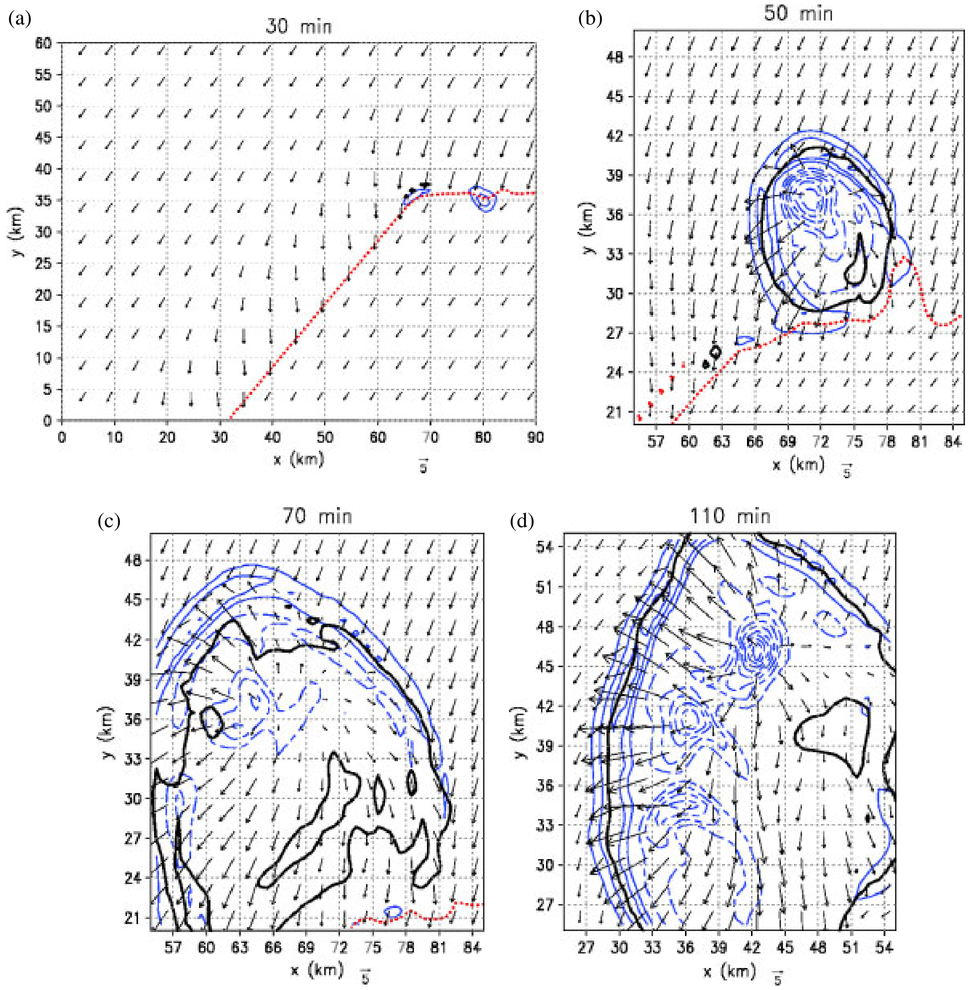

Figure 5. As Figure 4, but showing the low-level storm structure. Vectors represent the horizontal flow at the surface, and the surface divergence and convergence are contoured dashed and solid, respectively, at $2 \times 10^{-3}\,s^{-1}$ intervals, with the zero contour omitted. This figure is available in colour online at wileyonlinelibrary.com/journal/qj

In two further experiments we take the basic experiment, but with the position of the initial convection changed: in Experiment 5, convection is triggered ahead of the northerly sea breeze, and in Experiment 6 it is triggered behind this sea breeze.

By comparing Experiments 1–6 with the basic experiment, it is possible to answer the following questions:

- Does the orientation of the sea breeze(s) and the location of the initial cell relative to the sea-breeze front have an influence on the characteristics of the initial updraught (strength $w_{max,i}$, evolution with time)?
- How do the downdraught and gust front behave, and how strong are they in the different experiments?
- Is there new cell development on the gust front of the initial updraught, and
- Under what conditions does a large multicell storm form with more than three new cells?

The experiments are listed in Table I, together with their corresponding parameters and outcomes. In all experiments, the calculated CAPE is 4129 J kg^{-1} ahead of the sea-breeze air and 3517 J kg^{-1} within it. Thus, the instability of the environmental profile is the same in all cases.

In the experiments where the warm bubble is located ahead of the sea-breeze front (i.e. all except Experiment 6), the convection is triggered by an 8 km wide, 1 km deep, and 2 K warm thermal. However, in Experiment 6, the sea-breeze environment does not allow convection to be triggered by this thermal, and thus the temperature excess $\Delta\theta$ is increased to 6 K. With $\Delta\theta = 6$ K, the strength of the resulting updraught is comparable to those in the other experiments, allowing a better comparison of the characteristics of the generated cold pool and the subsequent development. However, the characteristics of the *initial updraught* ($w_{max,i}$, q_n, timing) in Experiment 6 should not be compared directly with those of the other experiments, as they are sensitive to the warm bubble parameters chosen (Wissmeier, 2009).

Table I shows that in Experiment 6 and in that with no sea breeze (Experiment 1), no multicell complexes develop. In the experiments with a single sea breeze (Experiments 2 and 3), a multicell storm with two or three new cells is generated, while in the cases with two sea breezes (basic, Experiments 4 and 5), large multicell storms form (here, 'large' means more than three cells: Table I). The set of experiments will be discussed in detail in section 4.1.

Further sensitivity experiments were carried out using the Kessler warm-rain scheme instead of the ice microphysics scheme, and with a *moist* sea breeze having a water vapour mixing ratio 2 g kg^{-1} larger than that in the environment. However in both experiments the evolution

Table I. Experiments with the corresponding model settings and parameters.

Experiment	Basic	1	2	3	4	5	6
NWsb	√	–	–	√	–	√	√
Nsb	√	–	√	–	√	√	√
Wsb	–	–	–	–	√	–	–
Warm bubble position (x, y) (km)	(85,38)	(85,38)	(85,38)	(85,38)	(85,38)	(85,28)	(85,48)
$w_{\mathrm{max,i}}$ (m s^{-1})	28.0	24.0	27.8	23.4	28.5	24.4	26.5
$t_{w\mathrm{max,i}}$ (min)	48	38	38	38	48	38	30
$w^{\mathrm{cb}}_{\mathrm{min,i}}$ (m s^{-1})	–15.0	–12.7	–14.97	–13.0	–14.8	–13.1	–12.2
$\overline{w^{\mathrm{cb}}_{\mathrm{min,i}}}$ (m s^{-1})	–10.2	–8.4	–10.2	–9.2	–10.0	–9.8	–7.7
$\max(q_n)$ (g kg^{-1})	17.5	11.6	16.5	11.5	18.2	12.0	13.0
t_{gf} (min)	42	42	42	42	42	42	36
$\overline{\lvert\partial u/\partial x + \partial v/\partial y\rvert}$ (10^{-3}s^{-1})	7.2	5.5	6.9	7.1	7.1	7.8	5.4
Time (min) of formation of the							
1st new cell	66	–	72	66	66	62	–
2nd new cell	72	–	76	76	68	72	–
3rd new cell	76	–	134	–	72	72	–
4th new cell	84	–	–	–	86	74	–
5th new cell	104	–	–	–	94	92	–
6th new cell	128	–	–	–	106	–	–
Type/size of multicell storm	Large	None	Small	Small	Large	Large	None

See section 4.1 for definitions.

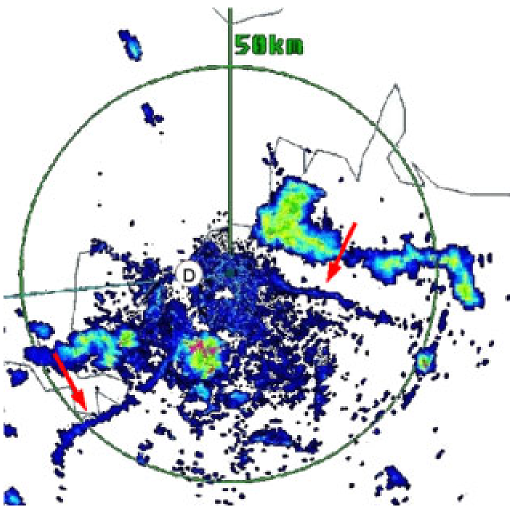

Figure 6. Berrimah radar image at 0420 UTC on 14 November 2005. The different shadings represent the reflectivity, where a reflectivity of 0 to −20 dBZ is shown as dark grey/black, and −20 to −65 dBZ in lighter shading. The city of Darwin is marked by D, and the arrows point to convective development at the sea-breeze fronts. Courtesy of the Australian Bureau of Meteorology Forecasting Centre in Darwin. This figure is available in colour online at wileyonlinelibrary.com/journal/qj

of the multicell storm, along with the new cell generation to the south of it, is similar to that in the basic experiment.

4.1. *Comparison of the seven experiments*

The results of the basic experiment and those of Experiments 1–6 are discussed in the following sections. This discussion centres on the time evolution of the maximum vertical velocity, $w_{\mathrm{max,i}}(t)$, the maximum downdraught velocity, $w^{\mathrm{cb}}_{\mathrm{min,i}}(t)$, at the cloud base level, the minimum horizontal divergence $(\partial u/\partial x + \partial v/\partial y)$ (i.e. maximum horizontal convergence) shown in Figure 7, and on the other pertinent results summarized in Table I. This table shows the different configurations of the sea breezes and the position of the warm bubble at the beginning of the simulations. It shows also the maximum vertical velocity of the initial updraught, $w_{\mathrm{max,i}}$, the time, $t_{w\mathrm{max,i}}$, at which the maximum is attained, the maximum downdraught velocity, $w^{\mathrm{cb}}_{\mathrm{min,i}}$, at the cloud base level, the average downdraught velocity, $\overline{w^{\mathrm{cb}}_{\mathrm{min,i}}}$, between the time of gust front occurrence, t_{gf}, and $t_{\mathrm{gf}} + 20$ min, and finally the mean low-level convergence $\overline{\lvert\partial u/\partial x + \partial v/\partial y\rvert}$, which is calculated between $t = t_{\mathrm{gf}} + 12$ min and $t = t_{\mathrm{gf}} + 20$ min. We compare now the results of the foregoing experiments based on the curves in Figure 7 and the data in Table I.

4.1.1. *Initial updraught*

Figure 7(a) shows clearly the growth and decay of the initial cell during the first 60 min followed by the development of the more severe stage of the storm, except in Experiments 1 and 6. Values of $w_{\mathrm{max,i}}$ lie between 23 m s^{-1} and 29 m s^{-1}. The smallest values are found in those cases where there was no sea breeze present (Experiments 1 and 3) or where the sea-breeze front was too far from the initial warm bubble (Experiment 5) to enhance the lifting of the bubble. The presumption here is that the sea breeze adds additional kinetic energy to the bubble in the lower atmosphere by augmenting the vertical perturbation pressure gradient at low levels.

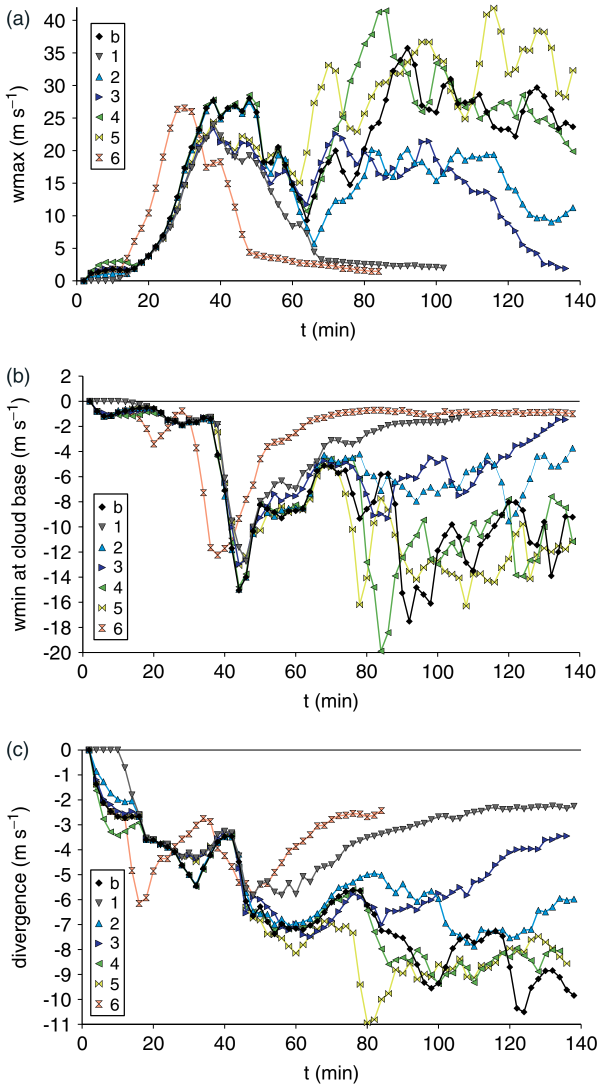

Figure 7. Timeseries of the (a) maximum vertical velocity, $w_{\rm max}$, (b) the minimum vertical velocity at cloud base, $w_{\rm min}^{\rm cb}$ ($z = 1.3$ km), and (c) the minimum in horizontal divergence, $\partial u/\partial x + \partial v/\partial y$, at $z = 190$ m (in $10^{-3}\,{\rm s}^{-1}$), measured over the whole horizontal extent of the domain. 'b' denotes the basic experiment, while the numbers 1 to 6 denote Experiments 1–6. This figure is available in colour online at wileyonlinelibrary.com/journal/qj

As seen in Table I, updraughts with large peak vertical velocities, $w_{\rm max,i}$, have correspondingly large maxima of hydrometeor mixing ratios, max(q_n), where q_n is the sum of the mixing ratios of cloud water $q_{\rm c}$, rain $q_{\rm r}$, snow $q_{\rm s}$, ice $q_{\rm ice}$, and hail/graupel $q_{\rm g}$. It is found that the peak in q_n occurs between $z = 4$ and 5 km and that $q_{\rm g}$ and $q_{\rm r}$ provide the largest contributions to max(q_n). Since updraughts hinder the fall-out of hydrometeors, strong updraughts can hold more hydrometeors aloft in the cloud and give them more time to grow via collision and coalescence than weaker updraughts. This effect explains the correlation between $w_{\rm max,i}$ and max(q_n).

4.1.2. *Downdraught and gust front*

Since the mid-tropospheric relative humidity and the vertical wind profile are the same in all the experiments, the entrainment of environmental air should have a similar effect on all the initial cells. Thus, differences in the downdraught strength are related mainly to the differences in ice and water loading (max(q_n)) within the storms.

The strength of the downdraught is characterized by the maximum downdraught velocity at the level of cloud base, $w_{\rm min,i}^{\rm cb}$, the time evolution of which is shown in Figure 7(b). Typically, the peak downdraught velocities occur about 6 min after the peak updraughts.

The amounts of ice and water loading are largest in the basic experiment and in Experiments 2 and 4, resulting in stronger downdraughts than in the other experiments. These strong downdraughts result in large gust-front speeds shortly after the cold pool forms (not shown). Thus, the presence or absence of a northerly sea-breeze front controls indirectly (via $w_{\rm max,i}$, max(q_n), $w_{\rm min,i}^{\rm cb}$) how strong the cold surface outflow of the initial cell will be *immediately* after the downdraught occurs. However, the updraught and downdraught strengths of the initial cell do not directly indicate whether a large multicell storm will develop *at later stages*. For example, in Experiment 5, a large multicell storm forms, while in Experiment 2 only three new cells develop on the gust front, even though the downdraught and subsequent cold pool are stronger at the beginning than in Experiment 5 (Table I).

4.1.3. *Convergence and new cell development*

The reason why the thunderstorm systems evolve differently in the different experiments is primarily a function of the strength and longevity of the low-level horizontal convergence.

In the foregoing experiments, the maximum low-level convergence is found at different locations along the gust front immediately after it forms. However, 12 min after the time of gust-front formation, the convergence is largest at the northwestern edge of the cold pool in all experiments except Experiment 6, where it is already largest in the northwest after 8 min (Figure 7(c)). This difference arises from the more rapid evolution of the initial updraught and gust front than in the other experiments because the initial warm bubble has a larger temperature excess.

The mean low-level convergence between 12 and 20 min after the gust-front formation is largest (typically 7–8 $\times 10^{-3}\,{\rm s}^{-1}$) in the experiments where a large multicell storm develops, i.e. in the basic experiment and in Experiments 4 and 5 (Table I). It is slightly smaller in the experiments where a small multicell storm develops (Experiments 2 and 3) and smaller still (maximum $5.5 \times 10^{-3}\,{\rm s}^{-1}$) in Experiments 1 and 6 in which there is no new cell development. Thus, in these experiments at least, the strength of the mean convergence at the gust front needs to exceed about $6 \times 10^{-3}\,{\rm s}^{-1}$ to trigger a new cell. Our calculations highlight the need also for the strong convergence to be present for a sufficiently long time. For example, in Experiments 1 and 6, the convergence is large immediately after the gust front forms, but subsequently decreases rapidly in strength (after 43 min in Figure 7(c)). As a result, the convergence weakens before new cell development is initiated.

The finding that strong convergence needs to be present for a sufficient time to initiate a new cell is supported by observations. In a study of the interaction between a southeastward-moving sea-breeze front and a northwestward-moving gust front from a pre-existing thunderstorm near Darwin, Keenan and Carbone (1992) noticed that a major new storm did not develop until 25 min after the collision of the fronts. A similar time lag was found also by Wilson and Schreiber (1986) in a study of midlatitude convection along boundary-layer convergence lines, where storms were initiated, on average, 19 min after the passage of the line.

The reason for the different convergence strengths at the gust front in the various experiments is related, of course, to the different model configurations. In three of the experiments with two sea breezes (the basic experiment, Experiments 4 and 5), there is enhanced convergence where the spreading gust front moves towards the sea-breeze flow, which is on the northwestern side of the cold pool (Figure 4(b)). A similar pattern of convergence occurs in Experiments 2 and 3 in which there is only one sea breeze. In these cases, the mean low-level convergence is slightly weaker. In Experiment 1, where there is no sea breeze, the convergence between the gust front and the environmental winds is not large enough to trigger new updraughts.

The question remains: why do we not see strong convergence, and thus new cell development, in Experiment 6, even though there are two sea breezes creating the same storm environment as in the basic experiment? The answer lies in the characteristics of the gust front, which opposes the environmental flow. The strength of the cold pool is determined by the strength of the downdraught, which is characterized by the time average of $w_{\rm min}^{\rm cb}$ over a 20 min period after the time of gust-front formation. In the basic experiment, the maximum downdraught velocity, $\overline{w_{\rm min}^{\rm cb}}$ is $-10.2\,\rm m\,s^{-1}$, while that in Experiment 6 is about 25% less. This difference in the mean downdraught strength is due to the larger temperature excess of the warm bubble in Experiment 6, which leads to a faster growth and decay of the cell and thereby to a weaker downdraught and gust front than in the basic experiment.

Note that the basic experiment was configured so that the storm development in the model resembles that which was observed on 14 November 2005. Thus, Experiment 6 shows that a warm bubble with $\Delta\theta = 6$ K initialized behind the northerly sea breeze cannot reproduce the Northeaster of this day. Nevertheless, this experiment is interesting because it shows that, without persistent strong low-level convergence, a multicell storm does not develop.

We examine now the location of secondary cell formation in the different experiments listed in Table I. In all but one experiment, the first new cell develops near the northwestern edge of the cold pool where the mean low-level convergence is largest. The one exception is that with the westerly and northerly sea breeze (Experiment 4), in which the first new updraught forms at the western edge of the gust front, where the convergence is smaller than in the northwest. This apparent inconsistency will be discussed in section 4.3, where the vertical forces are examined.

Of the 17 subsequent cells (2nd, 3rd, ...) studied, 76% of them form to the southwest of the previous updraught (Figure 4(d)). The reason for this organization is that the sea breezes, together with the low-and mid-level winds ahead of them, comprise an environment in which the low-level convergence is largest to the southwest of the previous cell. As the system evolves, the line of cells becomes oriented perpendicular to the low-level shear as seen in observations by Keenan and Carbone (1992). In two of the 17 cases, the convergence is not strongest at the location where the cells form. On the other hand, there are cases where, even though there is significant convergence, the secondary cell development does not occur. The comparison of the distances between neighbouring cells shows that a new updraught forms only at a distance larger than 5 km from pre-existing ones. This organization arises because subsidence from previous cells suppresses convection in their immediate vicinity (section 4.3).

Even though the initiation of convection by a density current in the form of a sea-breeze or gust front is primarily a function of the strength of the induced low-level horizontal convergence, there are several other factors that play a role in the initiation process. These factors have been studied theoretically and numerically in the past decades (Lafore and Moncrieff, 1989; Rotunno *et al.*, 1988; Weisman *et al.*, 1988; Weisman and Rotunno, 2004), but often only in two-dimensional configurations. The issues are discussed in the following sections.

It should be noted that the multicell storms and density currents in the model show significant three-dimensional features, which could potentially limit the applicability of two-dimensional theories to interpreting the overall system characteristics. Furthermore, the environmental shear profile of the 14 November 2005 case is neither idealized, nor is the shear concentrated at low levels. These properties may make it difficult to interpret the observations of the Northeaster and the model results obtained above in terms of the RKW theory.

4.2. *Vertical wind shear*

The overall evolution of a thunderstorm depends strongly on the vertical wind shear (e.g. Weisman and Klemp, 1982; Wissmeier and Goler, 2009; and references therein). In order to study the effect of the wind profile on the evolution of the Northeaster, the basic experiment is run with a uniform and unidirectional wind profile instead of the 14 November profile (section 4.2.1). The interaction between the environmental and cold-pool shear will be studied in section 4.2.2 in the light of the RKW theory.

4.2.1. *Tilting of the updraught*

The absence of vertical wind shear results in 79% stronger updraughts than in all the other experiments because of reduced entrainment. The strong updraughts and the large amounts of ice and water loading lead to intense downdraughts in the no-shear experiment, although the surface convergence at the leading edge of the cold pool is significantly smaller than that in the experiments where multicell storms develop. The reasons for this result are as follows. In the no-shear experiment, the gust front starts to decay about 10 min after the cold pool forms and no new cell develops. In contrast, in the cases where a second cell develops, the gust front is relatively strong for more than 20 min. The weak gust front in the no-shear case, and thus the relatively weak low-level convergence at the leading edge of the gust front, is due to the lack of strong tilting of the updraught as explained below.

The slope of the updraught is affected significantly by mid-tropospheric wind shear (Keenan and Carbone, 1991), as well as by the low-level shear that is generated by the cold-pool and/or sea-breeze density current(s). In the basic experiment, the northerly sea breeze and the environmental wind together lead to a tilt of the initial updraught towards

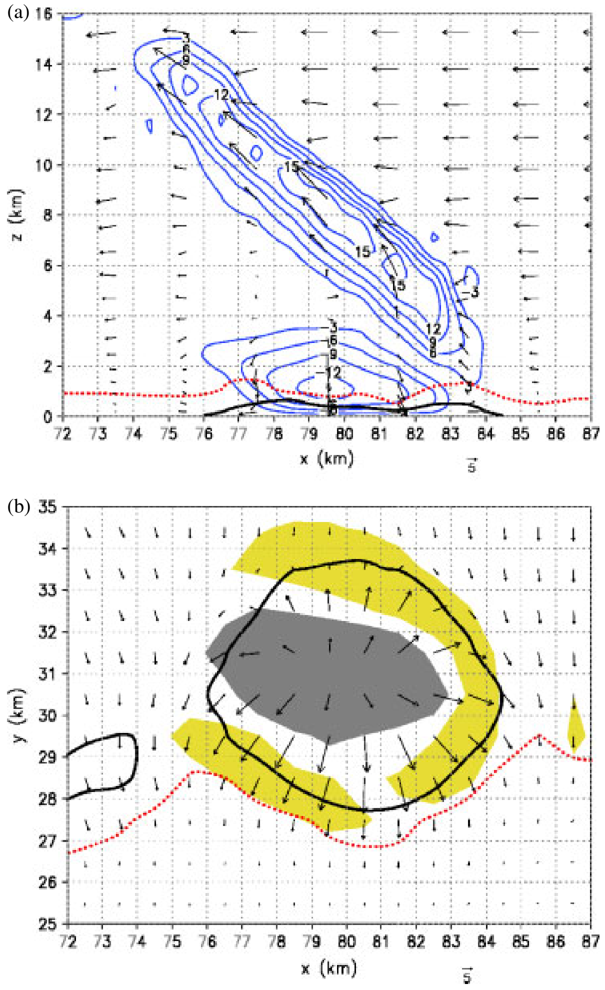

Figure 8. (a) Vertical cross-section at $y = 30.5$ km, and (b) horizontal cross-section at low levels through the initial updraught in an experiment with uni-directional wind shear. The sea-breeze front and the gust front are denoted by the bold dotted and solid lines, respectively. In (a), vectors represent the (u, w) flow, and w is denoted by the thin contours. In (b), vectors represent the (u, v) flow at $z = 0.06$ km, and regions of updraught velocities at cloud base larger than $2\ \mathrm{m\,s^{-1}}$ have light shading, while regions of $w < -2\ \mathrm{m\,s^{-1}}$ have dark shading. This figure is available in colour online at wileyonlinelibrary.com/journal/qj

the northwest. Accordingly, the downdraught is located to the northwest of the updraught, allowing it to supply the northwestern portion of the gust front continuously with cold air. In contrast, in the no-shear experiment, the initial updraught tilts only slightly towards the north in response to the horizontal vorticity generated by the northerly sea breeze. Then the downdraught falls into the updraught and rapidly weakens it. Further, without much tilt, the downdraught supplies air to the cold pool near its centre, more remote from the gust front than in the case with shear. As a result, the convergence near the gust front is too weak to generate secondary cells.

An example of a tilted updraught and its cold pool is shown in Figure 8(a) and (b). The initial updraught is tilted strongly towards the west, producing a downdraught to the west of the updraught base. As a result, the downdraught supplies the western portion of the cold pool with cool air (Figure 8(b)), while the storm-relative inflow from the east is able to supply the updraught with warm and moist environmental air (Figure 8(a)).

4.2.2. RKW theory

Despite the cautionary note above, we examine now the applicability of the RKW theory. Rotunno *et al.* (1988), Weisman *et al.* (1988), and Weisman and Rotunno (2004) showed that the ratio $c/\Delta u$ (Eq. (1)) is a useful parameter to characterize the structure and longevity of a squall line. While the choice of Δu for idealized unidirectional wind profiles is relatively straightforward, it is less clear-cut when the wind speed and direction vary with height, as is the case for the 14 November profile. Furthermore, because of the more complex flow configurations in Experiments 1 to 6 and the basic experiment than in the foregoing papers, c is more difficult to characterize with Eq. (2). This difficulty is due to the spatial variability of the buoyancy field. For these reasons, we apply a generalized RKW criterion by comparing the vorticity generated by the cold pool with that associated with the environmental vertical shear, which is modified at low levels by the sea breeze. These two quantities are characterized by the vertical differences in velocity behind the leading edge of the cold pool, and ahead of it, Δc_{pool} and Δc_{env}, respectively. Their ratio is given by the formula

$$\frac{\Delta c_{\text{pool}}}{\Delta c_{\text{env}}} = \frac{\|(u_2, v_2) - (u_1, v_1)\|_{\text{behind}}}{\|(u_2, v_2) - (u_1, v_1)\|_{\text{ahead}}} = \frac{\sqrt{(u_2 - u_1)^2 + (v_2 - v_1)^2}|_{\text{behind}}}{\sqrt{(u_2 - u_1)^2 + (v_2 - v_1)^2}|_{\text{ahead}}}, \tag{3}$$

where (u_2, v_2) is the wind vector at the top of the shear layer, $z = z_2$, and (u_1, v_1) is the wind vector at the base of it, $z = z_1$. Values of this ratio of order one are equivalent in the two-dimensional case to the RKW criterion.

There are conflicting views in the literature on the most appropriate depth of shear, $z_2 - z_1$, to use in the foregoing criterion. Rotunno *et al.* (1988) and Weisman *et al.* (1988) used a depth of 2.5 km, while Weisman and Rotunno (2004) found a better correspondence with overall squall-line structure when a 5 km shear depth was used. In the more complicated environment examined herein, the waters are fully uncharted. For this reason, we have calculated the environmental and cold-pool shears, Δc_{env} and Δc_{pool}, over three different depths: z_1 to z_2 = 0–1.1 km, 0–2.5 km, and 0–5 km (Table II), to determine which measure might be most appropriate.

The wind components used to calculate the shear ratio in Eq. (3) are determined at the location where the new cell develops at the time when the updraught exceeds $5\ \mathrm{m\,s^{-1}}$. This method differs from that of Rotunno *et al.* (1988), who calculate the undisturbed environmental shear at the beginning of the integration, without taking into account its local evolution as the storm develops. Since a multicell storm can have a significant influence on the local wind field, especially on the low-level shear (Lafore and Moncrieff, 1990), the vertical wind shear ahead of and behind the gust front is recalculated here each time a new cell develops. Figure 9(a) shows a horizontal cross-section through the storm system in the basic experiment at 98 min. Regions of upward motion at $z = 4.6$ km are shaded. The surface gust front is indicated by the thick black line and represents the –0.5 K temperature perturbation contour. Vectors represent the 0–1.1 km shear vectors. As can be seen in Figure 9(a), the second and third new updraughts develop in environments

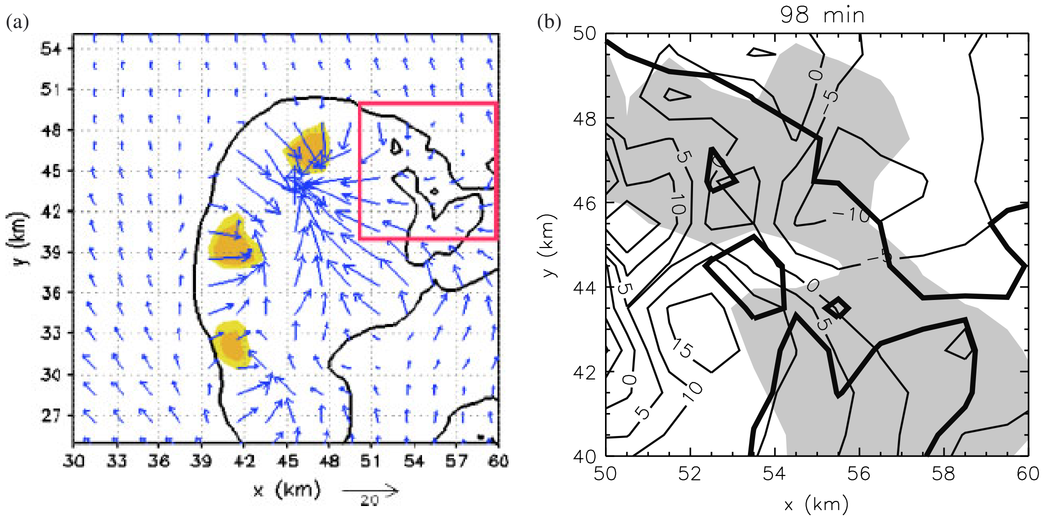

Figure 9. (a) Horizontal cross-section through the storm system in the basic experiment at 98 min. Regions of updraught velocity larger than $5\,\mathrm{m\,s^{-1}}$ at $z = 4.6$ km are shaded. The surface gust front is marked by the bold black line, which corresponds with the -0.5 K temperature perturbation contour. Vectors represent the 0–1.1 km shear vectors. (b) Net vertical force, PGF + B, at $z = 4.3$ km in the area marked by the box in (a). Contours are at $(-10, -5, 0, 5, 10, 15) \times 10^{-3}\,\mathrm{m\,s^{-2}}$, and the surface gust front is denoted by the bold black line and is oriented northwest–southeast. Regions of $w < -0.5\,\mathrm{m\,s^{-1}}$ are shaded. This figure is available in colour online at wileyonlinelibrary.com/journal/qj

where the angle between the environmental shear vector and the gust front is smaller than 90°. For the calculation of the shear ratio, only the components normal to the gust front are taken into account, since this component represents the central idea of RKW theory that the horizontal vorticity of the cold-pool shear should approximately balance that of the environmental shear for the updraught to achieve maximum development.

For the first new cell in the basic experiment, for example, a shear-ratio of 1.8 is obtained for depth 0–1.1 km when only the components of the two shear vectors normal to the gust front are considered. However, in most of the cases, the component of environmental shear normal to the gust front is very small, leading to shear ratios $\Delta c_{\mathrm{pool}}/\Delta c_{\mathrm{env}} \gg 1$. Table II shows these ratios calculated in the region of every new cell in the basic experiment and Experiments 2–5. The ratios are much larger than unity, indicating that the RKW criterion is not fulfilled in most of the cases. Thus, the complex flow configurations in Experiments 1 to 6 and the basic experiment make it difficult to predict the location of new cell development by examining the locations where $\Delta c_{\mathrm{pool}}/\Delta c_{\mathrm{env}} \approx 1$.

4.3. *Vertical perturbation pressure gradient and buoyancy*

To determine why no thunderstorms develop at the gust front, even though there is weak ascent at low levels, we consider the total vertical acceleration of air parcels given by

$$\frac{\mathrm{D}w}{\mathrm{D}t} = \underbrace{-\,c_p\theta_\rho\frac{\partial\pi'}{\partial z}}_{\mathrm{PGF}} + \underbrace{g\left(\frac{\theta_\rho}{\theta_{\rho0}} - 1\right)}_{B}, \tag{4}$$

where the two terms on the right-hand-side represent the vertical perturbation pressure gradient force (PGF), and the buoyancy force B. Here, g is the acceleration due to gravity, π' is the perturbation of the Exner function, π $(=(p/p^*)^\kappa$, where $\kappa = R/c_p)$, p is the pressure, p^* is the standard pressure (= 1000 hPa) and θ_ρ is the density potential temperature given by

$$\theta_\rho \equiv \theta\,\frac{1 + q_{\mathrm{v}}/\epsilon}{1 + q_{\mathrm{t}}}, \tag{5}$$

where q_t is the sum of the mixing ratios of water vapour q_{v}, cloud water q_{c}, rain q_{r}, snow q_{s}, ice q_{ice}, and hail/graupel q_{g}, and $\epsilon = R_{\mathrm{d}}/R_{\mathrm{v}}$ (gas constants for dry and water vapour, respectively). The inverse of θ_ρ is proportional to the density with the contribution of condensate loading included (Emanuel, 1994).

Figure 9(b) shows the net vertical force PGF + B in Eq. (4) in a region to the east of the first new cell of the basic experiment. In this area, the net force is negative at the gust front. This region where (PGF + B) < 0 partially overlaps with an area of subsidence caused by the first new updraught. The sinking motion depresses new cell formation at the northnortheastern edge of the gust front, even though there is weak ascent at low levels.

The foregoing calculations indicate that low-level convergence is not sufficient to determine whether new cells will be initiated. An example is the case of Experiment 4, where the first new cell is generated at the western edge of the cold pool, even though the surface convergence is larger at the northwestern edge. Figure 10 shows the net vertical force and the vertical velocity component in a region incorporating the westerly and northerly sea-breeze fronts. At 62 min, the vertical acceleration is largest in the west, ahead of the gust front where the net vertical force is positive. This force leads to the formation of the first new cell after 66 min, at (x, y)=(54 km, 34 km). Thus, in Experiment 4, the westerly sea breeze creates larger low-level instability at the western edge of the cold pool than at the northwestern edge.

The development or suppression of convection that could not be explained by considering the low-level convergence (section 4.1.3) is clear when the vertical force field and the vertical velocity component are considered.

Table II. Shear ratios $\Delta c_{pool}/\Delta c_{env}$ according to Eq. (3), between the environmental and cold-pool shear vector, for all experiments with new cell formation.

Experiment	0–1.1 km	0–2.5 km	0–5.0 km
All	7.2 ± 11.7	3.6 ± 6.7	4.2 ± 4.3
Basic	13.1 ± 21.4	4.8 ± 7.7	1.9 ± 1.3
2	4.8 ± 6.0	0.8 ± 0.5	6.0 ± 7.6
3	2.8 ± 1.2	1.1 ± 1.1	1.6 ± 0.0
4	6.9 ± 3.6	5.6 ± 10.3	6.2 ± 4.8
5	3.6 ± 4.7	2.3 ± 2.6	4.5 ± 4.4

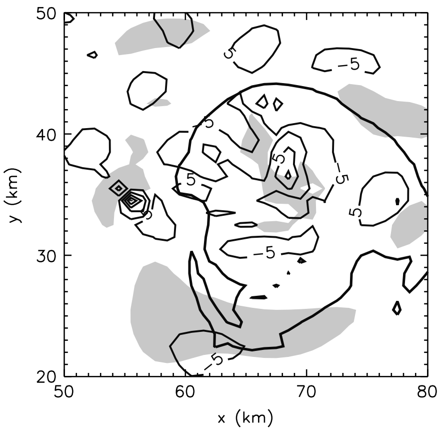

Figure 10. The net vertical acceleration, PGF + B, at $z = 4.3$ km, with contours at $(-5, 5, 15, 25, 35, 45) \times 10^{-3}$ m s^{-2}, and $w < -0.5$ m s^{-1} (shading), 62 min after the initialisation of Experiment 4. The surface gust front is denoted by the bold black line.

4.4. *Multicell thunderstorm at later stages*

At the time the multicell storm develops, the tilt of the individual cells is weak. However, the degree of tilt changes significantly as the cold pool and the multicell storm propagate towards the west. In the basic experiment, the gust front advances more rapidly than the individual cells of the multicell thunderstorm, with a relative speed of about 5.6 m s^{-1}. This rearward movement of the updraughts is accompanied by a tilting of the cells towards the east (Figure 11), which becomes progressively stronger with time. Because of the slope of the cells, the downdraughts and the regions of subsidence are located east of the updraughts. A similar behaviour was found also by Lafore and Moncrieff (1989). In their numerical study of the organization and interaction of convective regions of tropical squall lines, they estimated a forward movement of the cold pool exceeding that of the convective cells of about 10 m s^{-1}. In one of their model runs, the slope of the squall-line system changed when the distance between the gust front and the cells exceeded about 30 km. As a result, the 'rotor circulation' in the density current became stronger (Lafore and Moncrieff, 1989, Figure 9).

In the model, the Northeaster formed after 30 min and survived until the end of the simulation (3 h). The observed storm was equally long-lived: radar imagery showed it to be 25 km west of Darwin 2.5 h after its formation.

5. Summary and conclusions

Multicell thunderstorms such as the Northeasters that occur in the Darwin region of northern Australia have been simulated using an idealized numerical model. The evolution of a particular observed storm system was reproduced well in that, behind the sea-breeze fronts, new cells developed on the gust front of the initial updraught and formed a storm complex with similar characteristics to those observed, including propagation speed and direction, orientation, and length of the line of thunderstorms. Sensitivity experiments, with changes to the initial model configuration showed the following:

- A sea breeze can enhance the kinetic energy of the initial warm bubble leading to a stronger updraught, to more precipitation loading within the thunderstorm, and to a stronger downdraught and gust front than if there were no sea breeze or one were located far from the initial cell.
- A strong updraught and downdraught produced by the initial cell are not indicators as to whether a multicell thunderstorm will develop. Large low-level horizontal convergence is the primary factor determining the locations along the gust front of the initial updraught where new cell development is most likely, but it is not always a sufficient requirement.
- The low-level convergence at the edge of the cold pool should be strong and persist for a sufficient time for new cells to develop. This finding is consistent with observations of Keenan and Carbone (1992) and Wilson and Schreiber (1986) who noticed a time lag of about 19 min after the passage of a low-level convergence line before the formation of new cells.
- A generalized form of the RKW criterion was used to test whether the new updraughts developed at locations where the cold-pool circulation was largely opposed by that of the environmental shear. The comparison of the shear components normal to the gust front showed that new cells develop even though the RKW criterion is not fulfilled. Thus it would appear that the RKW criterion is not applicable to the more complex flow configurations studied here.
- The gust front is strong if the initial updraught is tilted sufficiently so that the downdraught does not fall into it, but supplies the cold pool continuously with cool air in the vicinity of the gust front.
- Updraught tilt is caused by strong environmental wind shear and by the horizontal vorticity generated by the sea breeze(s).
- Even though the convergence at the gust front is strong, the initiation of new cells can be suppressed by subsidence from pre-existing neighbouring cells.

The aim of this work has been to provide a deeper understanding of the evolution of the Northeasters and of

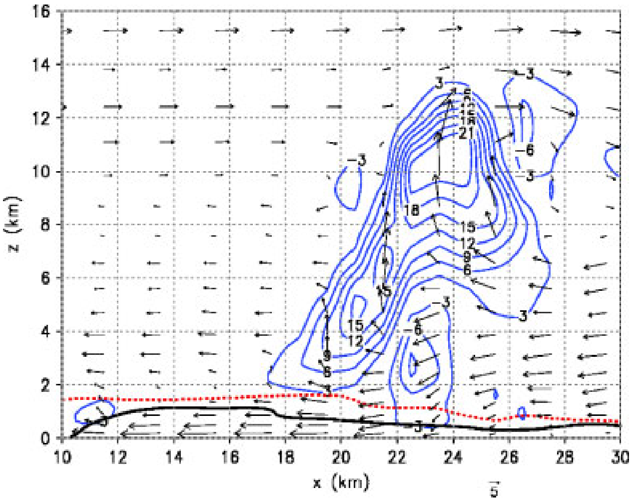

Figure 11. Vertical cross-section at $y = 34$ km through one of the cells of the multicell system in the basic experiment at 130 min. The sea-breeze front and the gust front are denoted by the bold dotted and solid lines, respectively. Vectors represent the (u, w) flow, and w is denoted by the thin contours. This figure is available in colour online at wileyonlinelibrary.com/journal/qj

the factors which lead to the development of thunderstorms with squall-like characteristics. Even though the experiments were motivated specifically by storms in the Darwin area, the basic principles and findings itemised above are expected to apply also to other regions in the Tropics and midlatitudes.

This study provides a basis for the future development and improvement of techniques for forecasting thunderstorms. For example, one of the major findings here is that sea breezes play a significant role in determining whether a severe multicell storm forms. When the sea-breeze flow opposes that of a gust front, the low-level horizontal convergence is enhanced and new thunderstorms are triggered along the gust front. Thus, it is of the utmost importance to determine whether and when sea breezes occur. Mesoscale models such as the Pennsylvania State University/National Center for Atmospheric Research Mesoscale Model (MM5) or the Weather Research and Forecasting model (WRF) could be used to forecast sea breezes and thus can improve the forecast of multicell storms such as the Northeaster.

Another important finding is that the updraught tilt is of the utmost importance to the development of a storm system. The slope of an updraught can lead to large horizontal convergence at a location where cold air from the downdraught is supplied to the gust front. Of course, not all parameters investigated in this study are available to the forecasters. In principle, the vertical tilt of a thunderstorm cell can be determined using radar reflectivity data, even though one must proceed with caution since storm movement and spatial resolution might affect the estimated tilt (Todd Smith, personal communication). If the amount and direction of tilting of a thunderstorm cell can be estimated, the region with the largest horizontal convergence at the edge of the cold pool, where new cell development is most likely, can be determined.

Acknowledgements

The authors express their gratitude to George Bryan for kindly making his numerical model available for this study and to Todd Smith at the Regional Forecasting Centre of the Australian Bureau of Meteorology in Darwin and Michael Foley at the Bureau's Head Office in Melbourne who drew our attention to this important problem and provided the observational data used. The first author acknowledges financial support from the German Research Council (Deutsche Forschungsgemeinschaft).

References

Bolton D. 1980. The computation of equivalent potential temperature. *Mon. Weather Rev.* **180**: 1046–1053.

Bryan GH. 2002. 'An investigation of the convective region of numerically simulated squall lines'. PhD thesis, Pennsylvania State University, USA.

Bryan GH, Fritsch JM. 2002. A benchmark simulation for moist nonhydrostatic numerical models. *Mon. Weather Rev.* **130**: 2917–2928.

Carbone RE, Wilson JW, Keenan TD, Hacker JM. 2000. Tropical island convection in the absence of significant topography. Part I: Life cycle of diurnally forced convection. *Mon. Weather Rev.* **128**: 3459–3480.

Emanuel KA. 1994. *Atmospheric convection*. Oxford University Press: Oxford, UK.

Gilmore MS, Straka JM, Rasmussen EN. 2004. Precipitation and evolution sensitivity in simulated deep convective storms: comparisons between liquid-only and simple ice and liquid phase microphysics. *Mon. Weather Rev.* **132**: 1897–1916.

Keenan TD, Carbone RE. 1992. A preliminary morphology of precipitation systems in tropical northern Australia. *Q. J. R. Meteorol. Soc.* **118**: 283–326.

Kingsmill DE. 1995. Convection initiation associated with a sea-breeze front, a gust front, and their collision. *Mon. Weather Rev.* **123**: 2913–2933.

Lafore JP, Moncrieff MW. 1989. A numerical investigation of the organization and interaction of the convective and stratiform regions of tropical squall lines. *J. Atmos. Sci.* **46**: 521–544.

Lafore JP, Moncrieff MW. 1990. Reply (to comments on Lafore and Moncrieff, 1989). *J. Atmos. Sci.* **47**: 1034–1035.

Lin YL, Farley RD, Orville HD. 1983. Bulk parameterization of the snow field in a cloud model. *J. Climate Appl. Meteorol.* **22**: 1065–1092.

May PT, Jameson AR, Keenan TD, Johnston PE, Lucas C. 2002. Combined wind profiler/polarimetric radar studies of the vertical motion and microphysical characteristics of tropical sea-breeze thunderstorms. *Mon. Weather Rev.* **130**: 2228–2239.

Rao PA, Fuelberg HE. 2000. An investigation of convection behind the Cape Canaveral sea-breeze front. *Mon. Weather Rev.* **128**: 3437–3458.

Rotunno R, Klemp JB, Weisman ML. 1988. A theory for strong, long-lived squall lines. *J. Atmos. Sci.* **45**: 463–481.

Wapler K, Lane TP. 2010. A case study of offshore convective initiation by interacting land breezes near Darwin, Australia. *Mon. Weather Rev.* submitted.

Weisman ML, Klemp JB. 1982. The dependence of numerically simulated convective storms on vertical wind shear and buoyancy. *Mon. Weather Rev.* **110**: 504–520.

Weisman ML, Klemp JB. 1984. The structure and classification of numerically simulated convective storms in directionally varying wind shears. *Mon. Weather Rev.* **112**: 2479–2498.

Weisman ML, Rotunno R. 2004. 'A theory for strong long-lived squall lines' revisited. *J. Atmos. Sci.* **61**: 361–382.

Weisman ML, Klemp JB, Rotunno R. 1988. Structure and evolution of numerically simulated squall lines. *J. Atmos. Sci.* **45**: 1990–2013.

Wilson JW, Schreiber WE. 1986. Initiation of convective storms at radar-observed boundary-layer convergence lines. *Mon. Weather Rev.* **114**: 2516–2536.

Wissmeier U. 2009. 'The physics of tropical convection'. PhD thesis, University of Munich, Germany.

Wissmeier U, Goler R. 2009. A comparison of tropical and mid-latitude thunderstorm evolution in response to wind shear. *J. Atmos. Sci.* **66**: 2385–2401.

